

Dynamic behavior of aluminum alloy plates with surface cracks subjected to repeated impacts

Fangjuan Duan^a, Jingxi Liu^{a,b*}, Ge (George) Wang^{c,d}, Zhaolong Yu^{e,f}

^aSchool of Naval Architecture and Ocean Engineering,

Huazhong University of Science and Technology, Wuhan 430074, China.

^b Collaborative Innovation Center for Advanced Ship and Deep-Sea Exploration(CISSE), Shanghai 200240, China

^c Research Center of Collision and Grounding, Zhenjiang 212003, China

^d gMarine, Houston TX 77024, gw.66@yahoo.com

^e Center for Autonomous Marine Operations and Systems (AMOS), Norwegian University of Science and Technology (NTNU), Norway

^f Department of Marine Technology, Norwegian University of Science and Technology (NTNU), Norway

Highlights

- The dynamic response of aluminum alloy plates repeatedly impacted by a rigid impactor has been investigated experimentally and theoretically.
- The permanent deformations of an impacted plate increase with each additional impact, and reach the largest values when the surface crack reaches the other side of the plate.
- The load-carrying capacity of a plate with a surface crack is sensitive to the crack length especially when the crack is shorter than the impactor diameter.
- The load-carrying capacity of a plate with a surface crack is also sensitive to the depth of the surface crack.
- Within the scope of the test program, the surface cracks had rather moderate influences on the permanent deformations.
- The analytical formulae of Jones was modified with the stresses determined based on the true stresses. Discussions were also given to some assumptions in this refined analytical formula.

* Corresponding author: liu_jing_xi@hust.edu.cn

Dynamic behavior of aluminum alloy plates with surface cracks subjected to repeated impacts

Abstract

This paper investigates the behavior of aluminum plates with and without initial cracks under repeated impacts. Three series of repeated impact tests were conducted to study the behaviors of circular plates that do not have any cracks (series B), have surface cracks with varying length (series L), and have cracks varying depths (series D). A hammer was dropped from the same height with a constant initial striking energy 60J for all tests. For each test specimen, the hammer was dropped nine times to simulate the scenario of repeated impacts. It was observed that plates with larger cracks carried smaller impact forces and assumed larger deformations. When the crack length was larger than the diameter of impactor, the responses of aluminum alloy plates became less sensitive to the crack length. With the increase in impact number, the effects of crack lengths and depths on dynamic behavior of aluminum alloy plates became much more significant. Predictions using a rigid-plastic theoretical model were compared with these test results, and discussions were given to the assumptions of this theoretical model. With the stresses determined based on the true strain-stress curve obtained by standard tension test, the refined analytical formula provides better predictions that agree well with the lab tests.

Keywords: Aluminum plates; Repeated impacts; Permanent deformation; crack size.

1. Introduction

During their lifespans, a ship's or an offshore platform's structures may be exposed to repeated impact loads, such as violent water slamming or green water, continuous ice floe impacts, dropped objects, etc. In general, a plate would accumulate more plastic deformations after each additional impact, and would carry ever larger impact loads with the increase in the number of impacts up to the point that the plate fails by cracking (Jones 2014b; Zhu et al. 2018). No design guidance for shell plating explicitly defines the structural limit states when the structure is subjected to repeated impacts. Often, a modern design code specifies a notional design load corresponding to a certain probability of occurrence for the intended design life, and requires the shell structure be designed not to fail by yielding or by not exceeding a limit of the permanent deformations (Wang et al. 2002). This design approach is based on an embedded assumption that came from the knowledge about the behavior of metal plates seldom re-visit for decades (Wang et al. 2006).

Research on a plate's dynamic behavior subject to repeated impacts dates back to the 1960's when the offshore oil and gas exploration was booming (Jones 1973). Jones (1977) proposed an analytical solution for predicting the permanent deformations of a rectangular plate under dynamic slamming pressure pulses. In his later research, the theoretical analysis for plating is extended for multiple mass impacts (2014b). Huang et al. (2000) proposed an energy criterion based on their own experimental and theoretical studies, and concluded that the elastic strain energy absorbed in the structure also increased with the increase in the plastic deformations. Zhu et al. discussed a variety of repeated impact scenarios that involved steel plates (1996) and aluminum foam sandwich plates at room and low temperature (2018). They showed again that with the increase in the number of impacts, both the impact forces and permanent deformations increased. Cho (2014) and Dac et al. (2017) investigated repeatedly impacted steel beams and concluded that the incremental permanent deformations decreased with the increase in the number of impacts. Cesim et al. (2015) conducted tests on glass/epoxy composites under repeated impacts, Onur et al. (2017) on repaired honeycomb sandwich structures, and Quang et al. (2018) on large-diameter, thin-walled stringer-stiffened steel

cylinders. In order to assess the load-capacity of ship side structures or bottom, a large number of experiments, analytical methods and finite element simulations have been conducted (Paik 2007a; Paik 2007b; Paik and Won 2007; Haris and Amdahl 2012; Storheim and Amdahl 2017; He 2016; Liu 2017).

In spite of these studies, the behavior of metal plates subject to repeated remains less investigated and there is a lack of test data available in the public domain.

Recently, there is a growing interest in understanding the effects of cracks on the (residual) ultimate strength of plates, stiffened panels or pipes. Cracks may occur during fabrication, operations, or, could be initiated by corrosion or a collision/impact. Relevant studies were often on their buckling behavior and their ultimate strength (Kumar 2004). A general expression of the ultimate strength of transversely cracked plates was derived based on the experimental and numerical results (Paik et al. 2005). Paik (2008, 2009) investigated the ultimate strength of plates with an initial longitudinal crack under axial compression using experiments and numerical simulations. The crack was parallel to the axial loading direction. Results showed that the longitudinal crack caused less reduction of load-carrying capacity than that with an initial transverse crack. The ultimate strength of structures with initial cracks was also studied by Seifi et al. (2011) for thin aluminum alloy plates, and for stiffened and unstiffened plates with varied crack position, length and angle between the loading direction and crack (Margaritis et al. 2012; Xu et al. 2014; Bayatfar et al. 2014; Rahbar et al. 2015; Shi et al. 2017). Hakan et al. (2015) investigated the effects of multiple initial surface cracks, through-thickness cracks and holes on the fracture and fatigue crack propagation of plates. In addition, the dynamic behavior of pipes with different initial crack shape and sizes were investigated (Zhang et al. 2018; He et al. 2018). The authors are not aware of any tests in the public domain that were devoted to cracked plates subjected to repeated impacts.

This paper summarizes a series of lab tests on aluminum plates with surface cracks under repeated impacts. Aluminum alloy has been extensively utilized in the construction of high-speed vessels and other lightweight structures because of its high strength over weight ratio and its strong resistance to corrosion (Burak 2017). The present research work is aimed to investigate the sensitivity of circular aluminum plates to initial cracks. The main objective has been to experimentally examine the residual ultimate strength characteristics of aluminum alloy plates with initial surface cracks under repeated impacts, where the depths and lengths are varied.

In this study, a rigid hammer with a round nose was raised to a pre-determined height and was dropped to strike aluminum plates at the location of cracks. The crack length and depth were varied to investigate their influences on the force-displacement curves and permanent deformations of specimens. Measurements were taken of deformations, force, number of impacts to rupture. Test of such nature is limited in the public domain, and the intent of this paper is to provide test data which can help better understand the loads and deformations of plates subject to repeated loads. This paper also presents predictions using a theoretical model and discusses assumptions used in this model.

2. The tests

2.1 The material

The aluminum alloy AA5083-H116 was utilized in this study. The prepared intact and cracked specimens have the same dimensions of 100mm×100mm×6mm, and they all were cut out from an aluminum alloy panel of 1000mm×1000mm×6mm.

In order to obtain their mechanical properties, standard tensile tests were carried out on coupons cut from the same aluminum panel, as is shown in Fig. 1. A representative engineering stress-strain curve and the corresponding true stress-strain curve are plotted in Fig. 2(a). The fitting curve of true stress at plastic stage is compared with some tensile test data points in Fig. 2(b). The mechanical properties are summarized in Table 1.

2.2 The specimens

A total of thirty identical test specimens were cut from the same parent aluminum plate. They were 100 squares with a thickness of 6mm. Fig. 3 shows a photo of one such test specimen. Each specimen was fastened to the strong support/clamp frame through 12 bolts. As the support frame has a circular opening in the middle 75mm in diameter, the test specimens should be considered as circular plates with a diameter of 75mm.

A total of ten series of tests were conducted with three identical specimens in each test. Table 2 summarizes these tests. The characters of R and H represent the radius of the impactor head (6mm) and thickness of specimens (6mm), respectively.

Test series B was to provide base cases for the entire program. Specimen B0 was an intact plate without initial cracks. Specimens B-1 had the base case surface crack that is 8mm long and 1mm deep.

Test series L was designed to investigate the effects of crack length. The initial crack length remained the same at 1mm, and the crack length was varied. With the crack length $L=2, 4, 6, 8$ (Specimen B-1), 12 and 16mm, this test series covers the range of $L/2R$ ratio from $1/6$ to $4/3$.

Test series D was to investigate the effects of crack depth. The initial crack depth remained the same at 1mm, and the crack length was varied. Two additional crack depths were made, one with a depth of 3mm and the other 6mm (a through-thickness crack). The D/H ratio ranges from $1/6$ to 1.

2.3 The crack

Cracks were prefabricated with an electrical discharge machining (EDM) system. EDM is a useful machining process widely applied in machinery industries for several decades. Key advantages are the absence of a cutting force and the flexibility for machining. Haddad et al. (2010) showed that EDM could machine materials with small-size features and high precision. Although EDM leads to the thermal loads in the workpiece material which may cause mechanical property modification, Liu et al. (2016) found that the temperature decreased significantly to a low value within the depth of $20\mu\text{m}$, which is rather small compared to the thickness of specimens in this paper. Therefore EDM is a feasible solution for machining surface cracks in this paper having varied lengths and depths with a strict precision requirement.

The tool electrode material is forged commercial pure copper with a density of 8933 kg/m^3 . The tool electrode does one-way movements at constant speeds in vertical and horizontal direction with 0.03mm accuracy. The final position of tool electrode on the Z-axis determines the depth of the crack. The horizontal feed distance on X-axis determines the length of the crack. The deionized water is supplied continuously to cool and flush debris away from the gap. The overall layout of fabrication is shown in Fig. 4. The detailed machining process is shown in Fig. 5. After the completion of the prefabricated crack, the specimen is cleaned with gasoline and other solvents. A dryer is used to take away the residual fluid on the surface and in the crack. The specimen with a prefabricated crack of 8mm length is shown in Fig. 3.

2.4 The impact by dropping a hammer

Figure 6 shows the test rig. The impact was realized by releasing the hammer from a pre-selected height and hitting the specimen at a controlled speed. The hammer aimed at the center of the specimens which is also the location of the surface crack. The surface cracks were on the lower surface of the specimen, opposite to the hammer. To prevent the rebound hammer from hitting the specimens twice in one hammer dropping, a rebound catcher was installed. In the consequential hammer droppings, the hammer was released from the same height and hit the specimens at exactly the location. This would ensure that the specimens were subject to repeated impacts of a same energy.

The hammer was made of forged steel totally weighted 13.26kg, and had a hemispherical head 12mm in diameter. The energy used in this study was selected as 60J to trigger perforation of specimens after a few repeated impacts.

The test specimens were bolted to two clamping frames, which were 10mm thick steel plates. Figure 7 shows this clamping arrangement and Fig. 3 shows the locations of the twelve bolts on each specimen. This arrangement would allow virtually no rotation, axial or lateral movement of the specimens along their edges.

2.5 The measurements

The impactor and force transducer were connected to a crosshead to measure the contact force between the impactor and specimen at a sampling frequency of 2MHz. The measured results including force-time, displacement-time and energy-time relation curves were obtained by computer with data acquisition system. After each hammer dropping, photos were taken of both the front surfaces and rear surfaces (with surface cracks). The rear surface was scanned using a laser displacement sensor along two marked lines that crossed at the center of the specimen (see Fig. 8)

3. Experimental results and discussion

3.1 Intact specimen under repeated impacts (Test B-0)

Figure 9 shows the time history of impact forces and force-displacement curves of Test B-0. The specimens were perforated after 9 repeated impacts. As impacts repeated, the contact force increased significantly while the impact duration decreased. After 6 repeated impacts, the maximum force started to decrease. This coincided with the occurrence of metal rupture at the 6th impact. Finally, the aluminum alloy plates failed as a result of front surface tensile failure or matrix cracking on the indented circle. Permanent deformations increase continuously until perforation. As the impact number increases, the increment of displacement decreases while the loading stiffness of each impact increased.

During the first impact, the loading slope is much smaller than that of the following repeated impacts. The reason is the formation of indentation, which leads to a larger increment of displacement. In the following impacts, the force-displacement curves show virtually identical loading and unloading stiffness in two consecutive impacts, and then the slopes decline in plastic stage. The closed area of the curve represents the absorbed energy by the specimen. In the last impact, there are three stages. Firstly, the impact force increases with displacement till the peak point, then drops suddenly due to the rupture of the rear surface. In the second stage, the impact force reaches a plateau, as the deflection of the specimen keeps increasing, implying that the damaged aluminum alloy plate still has certain load-carrying capacity after the rupture of the rear surface. In the last stage, the impact force decreases sharply due to the local perforation of the specimen with a small decrease of displacement for the releasing of elastic strain energy stored in the specimen.

The shape profiles of deformation after each impact of intact specimen are shown in Fig. 10. The corresponding damage profiles of the specimen after the first, the third, the sixth, and the ninth impact are plotted in Fig. 11. Evidently, the deformation of the specimen becomes larger with each additional impact. The plate center is directly pushed by the impactor thus has the maximum permanent deformation. The asymmetry of shape profile after the last impact is due to the perforation of the specimen.

The local dent conforms to the shape of the impactor head. Indentation grows continuously as the impacts continue, and so does the ratio of local indentation over total deformation. After several impacts, a necking circle formed due to the accumulated tensile strain. As impact continues, a crack initiates on the necking circle and quickly develops into a through-thickness crack, causing failure of the specimen.

3.2 Effects of initial crack length (Test L series)

The maximum impact forces of specimen with six different initial crack lengths (L) and a constant crack depth of 1mm under repeated impacts are summarized in Fig. 12. The crack length of 0mm stands for the intact specimen. It is observed that for the specimens with $L/2R$ less than 1, the number of impacts to rupture is 9, while this number becomes 8 for specimens with $L/2R$ of 1 and $4/3$. Compared with the intact specimen, a plate with a surface crack decreases the impact force, and longer cracks cause greater decrease in the impact forces.

As impact continues, the effect of $L/2R$ on impact force becomes much more pronounced. For the specimens with an $L/2R$ less than 1, the peak forces in repeated impacts appeared in the 6th impact, one time later than the specimens with $L/2R$ of 1 and $4/3$. It also can be seen that even a short initial crack can reduce the impact force significantly. However, when the crack length is larger than the impactor diameter, the effect of change in crack length is rather moderate. When $L/2R$ is less than 1, the aluminum alloy plates are sensitive to the initial crack length.

The impact force-displacement curves of specimen with different initial crack lengths at the selected impact numbers are compared in Fig. 13. Four out of six crack lengths are chosen to show in this figure. In the first impact, the impact force increases with milder stiffness compared to that in the later impact. In the following repeated impacts, **constant impact forces** occur. The values of peak force increase with impact number, and decrease due to the rear skin tensile failure after the 6th impact.

It is found that in the first impact, the force-displacement curves and permanent deflections are almost independent of $L/2R$. In the following impacts, for specimens with an initial crack length being equal or larger than the diameter of the impactor ($L/2R=1, 4/3$), the force-displacement curves show little difference. However, the influence becomes significant when initial crack length is less

than the diameter of the impactor ($L/2R=0, 1/3, 2/3$). In the 6th impact, the effect of initial crack length on the stiffness of the loading and unloading stage is much more significant than that in lower repeated number impacts. The difference values of peak force and permanent displacement among the specimens with different $L/2R$ increase significantly with impact number, due to the accumulation of impact energy. In the 8th impact, the difference of the stiffness becomes smaller but the effect of initial crack length on peak force and permanent displacement is still large.

Figure 14 shows damage evolution of specimens with different initial crack lengths. Compared with the damage of intact specimen in Fig. 11, an initial crack affects significantly the damage mode. Specimens with different $L/2R$ ratio would yield quite different modes in crack initiation and propagation. The damage modes can be divided into three types.

- For specimens with a short initial crack ($L/2R=1/6, 1/3$), the initial crack propagated along its length direction from both ends and then extended sideways, forming several new cracks. The new cracks initiated at the 6th impact, which explains why the peak force took place as shown in Fig. 12.
- For specimens with a moderate crack length ($L/2R=1/2, 2/3$), tensile cracks appear at both ends of the initial crack in the perpendicular direction due to the excessive tensile stress on crack tips. As the impact number increases, cracks propagated forward around the dent marks and finally caused the perforation of the specimens.
- For specimens with an initial crack equal to or longer than the impact diameter ($L/2R=1, 4/3$), the spherical impactor penetrates the specimens with ductile enlargement elongating the material below the impactor. When the specimens undergo considerable plastic strain, new tearing cracks appeared in a direction perpendicular to the initial crack. They started from the necking around the dent circle. Finally, the fractures propagated through the necking circle after 8 repeated impacts.

3.3 Effects of initial crack depth (Test D series)

Maximum impact forces of specimens with three different initial crack depths under repeated impacts are summarized in Fig. 15. D/H stands for the ratio of initial crack depth to specimen thickness. Especially, specimen with $D/H=1$ represents specimen with a through-thickness crack. The

number of impacts to rupture decreases with the increase in initial crack length, being 9, 8, 7 for D/H ratios of 1/6, 1/2 and 1, respectively. The peak force took place at the 6th impact when $D/H=1/6$ and 1/2, at the 5th impact for specimens with through-thickness crack. The effect of D/H on the impact force between specimens of $D/H=1/2$ and 1 becomes more significant with the impact number increasing.

Figure 16 shows the impact force-displacement curves of specimen with different crack depths during different impact cycles. All specimens show similar trend in the force-displacement curves. In the first impact, there is little difference in the peak value of impact force and permanent displacement between specimens with $D/H=1/2$ and $D/H=1$, while the peak force of specimen with $D/H=1/6$ is larger and the permanent displacement is smaller. A force platform occurs on the impact force-displacement curve after the 1st impact. As the impact number increases, displacements as well as differences of displacement among specimens with different crack depths increase. The peak value of impact force and the slope of force-displacement among specimens with different crack depths are close to each other in the 3rd and 5th impact. In the 7th impact, the influence of D/H on the permanent displacement and stiffness is much more significant than that in previous repeated impacts. The specimen with $D/H=1$ ruptures at the 7th impact, the impact force decreases after the peak point due to the opening of initial crack. Then a force platform occurs because of the residual load-carrying capacity of the specimen. Finally the curve of force-displacement drops drastically due to perforation.

The evolutions of damages with different initial crack depths are given in Fig. 17. It is easily observed that the damage of specimen with deeper initial crack is larger. The damage mode of specimen with $D/H=1/6$ is similar to that of specimen with $D/H=1/2$. As the impact number increases, the rear surfaces of the specimens open at the initial crack and the deflection of the front surfaces increase. When the cracks grow from the tip of initial crack and extend sideways, the deflection of the front faces rise rapidly. Finally cracks propagate to the front surface and the impactor perforates the specimens along the cracks. For the specimen with an initial through-thickness crack, the rear surface opens at the crack while the material at both sides of the crack on the front surface is compressed together under repeated impacts. As the impact number increases, cracks initiate at the end of the initial crack on the rear face, and the front face opens long these cracks till rupture of the specimen.

The rupture side images of specimens with different initial crack depths can be seen in Fig. 18. It is evident from the figures that the local indentation of specimens with different D/H shows big differences. The perforation of specimen with a small crack depth is the result of high tensile stress due to the forward motion of the plate material being pushed by the impactor. But for the specimens with a deeper initial crack, the material on both sides of the crack extended away gradually, the removal of material causes the discontinuity of membrane force which severely decreases the load-carrying capacity of the specimens.

4. Theoretical predictions

4.1 Maximum deformations of a circular plate under repeated impacts

Jones (2012a) proposed a solution for predicting the permanent deformations of a plate when subjected to large static or dynamic load. Later he extended his solution for multiple impacts. Most former researches used the first order or classical theory to study the plastic collapse behavior of ductile structures undergoing infinitesimal displacements. While under sufficiently large loadings, the response of beams and plates can change significantly. Jones studied the dynamic response and predicted the deformation of plates, which underwent moderate finite transverse displacements and induced membrane forces.

The motion of a perfectly plastic metal plate is governed by the following equation,

$$-G\ddot{w} - \mu\dot{w} = \mu C_m \dot{w} + \mu C_u \dot{w} \quad (1)$$

Where, G is the mass of impactor, μ is the mass per unit surface area of the plate, w , \dot{w} and \ddot{w} are the transverse displacement, the velocity and acceleration of the plate respectively, W is the transverse displacement at the plate center which is underneath the impactor. Eq. (1) ensures that the external work rate due to the inertia forces equals the internal energy dissipated at the plastic hinges and within the plastic zones.

The governing equation according to the method developed by Jones (2014a) for the dynamic response of a fully clamped, rigid, perfectly plastic circular plate can be written in the form

$$\ddot{v} = -\alpha^2 H \quad (2)$$

where

$$\alpha^2 = 6(\sigma_0/\rho a^2)(1+6\gamma)^{-1} \quad (3a)$$

$$\gamma = G/\rho H \pi a^2 \quad (3b)$$

Where, γ is the ratio of the impactor's mass to that of the metal plate.

The solution for Eq. (2) gives the dimensionless maximum transverse displacement,

$$\frac{W_f}{H} = \sqrt{1 + \frac{\Omega}{\pi}} - 1 \quad (4)$$

where,

$$\Omega = \frac{G V_0^2}{\sigma_0 H^3} \quad (5)$$

Jones (2014b) assumed that Eq. (2) remains valid for the following impacts of identical kinetic energy. After the n th impacts, the dimensionless permanent transverse displacement turns out to be,

$$\frac{W_m}{H} = \sqrt{1 + \frac{n\Omega}{\pi}} - 1 \quad (6)$$

Appendix gives the detailed solutions.

4.2 Comparison between theoretical predictions and experimental results

The experimental results of Test B-0 in Table 2 are compared with the theoretical predictions of Eq. (6) in Fig. 19. Four different stresses were assumed for presenting the aluminum's stress σ_0 in Eqs. (3) and (5). They are yield stress σ_y , true stress σ_t , flow stress σ_f and ultimate stress σ_u .

The true stress σ_t is obtained according to the real stress-strain curve of AA5083-H116 obtained from the coupon tests as shown in Fig. 1. Since the impactor has a small nose in comparison to the radius of the plate, the influence of the nose is very limited. The equation for the maximum plastic strain after each impact can be simplified to

$$\varepsilon = \sqrt{(W_m/a)^2 + 1} - 1 \quad (7)$$

Then, σ_t can be easily obtained from the real stress-strain curve in Fig. 2(b).

The flow stress σ_f of the plate is often taken as $\sigma_f = (\sigma_y + \sigma_u)/2$ (Jones 2012b; Zhang 2018; Hong 2009), where, σ_y and σ_u are the initial yield stress and the ultimate tensile stress, respectively.

4.3 Discussion and a refined analytical solution

The following observations from Fig. 19 are worth to mention:

- The assumptions of using σ_y lead to over-estimates of the permanent deformations, while predictions using σ_u under-estimate.
- The assumptions of the flow stress σ_f and true stress σ_t lead to better predictions of permanent deformations that agree well with the experimental data.

Assumption of the (initial) yield stress predicts the best result for the first impacts. This is expected because during the first impacts, the plates saw yielding in areas at proximity to the dropped hammer with no material's necking or rupture. With the increase in the number of impacts, more and more materials entered the plastic range, and the maximum strains in the plate became larger. As a result, predictions using the yield stress deviate more from the tests with each additional impacts.

Assumption of the ultimate stress σ_u for all impacts is apparently not valid. Rupture took place after a few impacts in a few locations at the vicinity of the impact location, while the majority of the plate remained not cracked. This indicates that ultimate stress only took place in some local areas and should not be used for representing the entire plate.

Using the true stress gives better agreement with the experimental data. Good comparisons are observed particularly for the first few impacts. Nevertheless, there exist discrepancies between tests and predictions. A main reason for the differences is that the Jones' analytical model assumes rigid-perfectly plastic material, which can't fully capture the curved geometry of the deformed plates as observed in Fig. 18.

Apparently, an improvement to the Jones (2014b) solution is to use the true stresses for

representing the material's post-yield stress. This refined solution is in Eqs. 6 and 7, which provide better estimates of the permanent deformations after each impact up to the point that material's rupture takes place.

As for the plates with surface cracks, the authors are not aware of any theoretical analyses. Figure 20 shows the test results of the L- and D-Series together with the predictions for intact plates using the refined analytical solutions. Apparently, the effect of the initial crack on the deformation is rather limited within the current scope of testing.

More attentions will be given to larger surface cracks in future experimental and numerical researches.

5 Conclusions

This paper reports an experimental study on the behavior of aluminum plates with surface cracks subject to repeated impacts. This experimental investigation is designed to represent the worst case scenario, although in reality repeating impacts may not take place at the same position on a structure.

The permanent deformations were also calculated using a refined theoretical model based on Jones (2014b), and discussions were given about how to accurately predict using analytical formulae.

The following conclusions may be drawn:

- (1) As the number of impacts increased, the deformations of the aluminum plates increased, the impact forces increased, the impact durations decreased, and the stiffness of the plate increased. The plates reaches the highest load-carrying capacity after the six impacts in almost all the test series, when the cracks became through-thickness.
- (2) With a longer crack, the impact forces reduced while the deformations increased. Plates with surface cracks are sensitive to the length of cracks when $L/2R$ is less than 1 (short cracks). With a deeper crack, the impact forces reduced while the deformations increased.
- (3) Both the effects of crack length and depth on the dynamic responses of aluminum alloy plates become more and more pronounced with the increase in impact number.
- (4) The formulae of Jones (2014b) can be refined by using the true stress for representing the

material's post-yield behavior. This refined analytical solution provides reasonable predictions of the maximum deformations that compare well with the lab tests. Careful consideration shall be given to how to select a proper stress for representing an aluminum plates after yielding takes place in the plate.

Acknowledgements

The present work is supported by National Natural Science Foundation of China (Grant No. 51579110) and the Fund project Independent Innovation Research Fund of Huazhong University of Science and Technology (Grant No. 2015TS004). The authors expressed valuable discussions with many colleagues over the course of test planning, result analyses, manuscript drafting.

References

- Bayatfar A, Khedmati MR, Rigo P. 2014. Residual ultimate strength of cracked steel unstiffened and stiffened plates under longitudinal compression. *Thin-Walled Struct.* 84(0):378–92.
- Burak Can Cerik. 2017. Damage assessment of marine grade aluminum alloy-plated structures due to air blast and explosive loads. *Thin-Walled Struct.* 110:123-132.
- Cesim A, Akar D. 2015. An experimental investigation on the repeated impact response of glass/epoxy composites subjected to thermal ageing. *Comp Part B.* 75:127-34.
- Cho SR, Dac DT, Hyun KS. 2014. Repeated lateral impacts on steel beams at room and sub-zero temperatures. *Int J Impat Eng.* 72:75-84.
- Dac DT, Hae-Jung J, Hyun KS, Sang-Rai C. 2017. Response of low-temperature steel beams subjected to single and repeated lateral impacts. *Int J Naval Archit Ocean Eng.* <https://doi.org/10.1016/j.ijnaoe.2017.10.002>.
- Haddad MJ, Alihoseini F, Hadi M, Hadad M, Tehrani AF, Mohammadi A. 2010. An experimental investigation of cylindrical wire electrical discharge turning process. *Int J Advanced Manufacturing Tech.* 46:1119-32.
- Hakan D, Ali OA. 2015. Three-dimensional fracture and fatigue crack propagation analysis in structures with multiple cracks. *Comput Struct.* 158:259-73.
- Haris S, Amdahl J. 2012. An analytical model to assess a ship side during a collision. *Ships Offshore*

Struct.7(4):431-448.

- He JZ, Wang GZ, Tu ST, Xuan FZ. 2018. Prediction of creep crack initiation behavior considering constraint effects for cracked pipes. *Eng Fract Mech.* 190:213-31.
- He WT, Liu JX, Tao B, Xie D, Liu JY, Zhang M. 2016. Experimental and numerical research on the low velocity impact behavior of hybrid corrugated core sandwich structures. *Compos Struct.*158:30-43.
- Hong L. 2009. Simplified analysis and design of ships subjected to collision and grounding [PhD thesis]. Trondheim: NTNU.
- Huang ZQ, Chen QS, Zhang WT. 2000. Pseudo-shakedown in the collision mechanics of ships. *Int J Impact Eng.* 24(1):19-31.
- Jones N. 1973. Slamming damage. *J Ship Res.* 17(2):80-6.
- Jones N. 1977. Damage estimate for plating of ships and marine vehicles. In: *International Symposium Practical Design in Shipbuilding (PRADS)*. Tokyo: Society of Naval Architects of Japan. p. 121-8.
- Jones N. 2012a. *Structural impact*. 2nd ed. Cambridge University Press: 584pp.
- Jones N. 2012b. Impact loading of ductile rectangular plates. *Thin-Walled Struct.* 50:68-75.
- Jones N. 2014a. Dynamic inelastic response of strain rate sensitive ductile plates due to large impact, dynamic pressure and explosive loadings. *Int J Impact Eng.* 74:3-15.
- Jones N. 2014b. Pseudo-shakedown phenomenon for the mass impact loading of plating. *Int J Impact Eng.* 65:33–9.
- Kumar YVS, Paik JK. 2004. Buckling analysis of cracked plates using hierarchical trigonometric functions. *Thin-Walled Struct.* 42(5):687-700.
- Liu JF, Gao YB. 2016. Thermal modeling of EDM with progression of massive random electrical discharges. *Procedia Manufacturing.* 5:495-507.
- Liu JX, He WT, Xie D, Tao B. 2017. The effect of impactor shape on the low-velocity impact behavior of hybrid corrugated core sandwich structures. *Compos Part B.*111:315-331
- Margaritis Y, Toullos M. 2012. The ultimate and collapse response of cracked stiffened plates subjected to uniaxial compression. *Thin-Walled Struct.* 50(1):157–73.
- Onur B, Onur Ç, Mustafa ÖB, Eyüp A, Enver BY. 2017. Experimental investigation of single and repeated impacts for repaired honeycomb sandwich structures. *Mater Sci Eng A.* 682:23–30.

- Paik JK, Kumar YS. 2005. Ultimate strength of cracked plate elements under axial compression or tension. *Thin-Walled Struct.* 43:237–72.
- Paik JK. 2007a. Practical techniques for finite element modeling to simulate structural crashworthiness in ship collisions and grounding (Part I: Theory). *Ships Offshore Struct.* 2(1):69-80.
- Paik JK. 2007b. Practical techniques for finite element modelling to simulate structural crashworthiness in ship collisions and grounding (Part II: Verification). *Ships Offshore Struct.* 2(1):81-85.
- Paik JK, Won SH. 2007. On deformation and perforation of ship structures under ballistic impacts. *Ships Offshore Struct.* 2(3):217-226.
- Paik JK. 2008. Residual ultimate strength of steel plates with longitudinal cracks under axial compression—experiments. *Ocean Eng.* 35(17–18):1775–83.
- Paik JK. 2009. Residual ultimate strength of steel plates with longitudinal cracks under axial compression—Nonlinear finite element method investigations. *Ocean Eng.* 36(3–4):266–76.
- Quang TD, Teguh M, Hyun KS, Cho SR. 2018. Dynamic lateral mass impact on steel stringer-stiffened cylinders. *Int J Impact Eng.* <https://doi.org/10.1016/j.ijimpeng.2018.02.007>.
- Rahbar-Ranji A, Zarookian A. 2015. Ultimate strength of stiffened plates with a transverse crack under uniaxial compression. *Ships Offshore Struct.* 10(4):416–25.
- Seifi R, Khoda-yari N. 2011. Experimental and numerical studies on buckling of cracked thin-plates under full and partial compression edge loading. *Thin-Walled Struct.* 49(12):1504–16.
- Shi XH, Zhang J, Soares CG. 2017. Experimental study on collapse of cracked stiffened plate with initial imperfections under compression. *Thin-Walled Struct.* 114:39-51.
- Storheim M, Amdahl J. 2017. On the sensitivity to work hardening and strain-rate effects in nonlinear FEM analysis of ship collisions. *Ships Offshore Struct.* 12(1):100-115.
- Wang G, Tang S, Shin Y. 2002. Direct calculation approach and design criteria for wave slamming of an FPSO bow. *Int J Offshore Polar Eng.* 12:297-304.
- Wang G, Wiernicki C. 2006. Using nonlinear finite element method to design ship structures for ice loads. *J Marine Tech.* 43(1):1-15.
- Xu MC, Garbatov Y, Soares CG. 2014. Residual ultimate strength assessment of stiffened panels with locked cracks. *Thin-Walled Struct.* 85:398–410.

Zhang Y, Lie ST, Zhao HS. 2018. Fracture behavior of clad pipeline containing a canoe shape surface crack subjected to large bending moment. *Marine Struct.* 58:92-108.

Zhang M, Liu JX, Hu ZQ & Zhao Y. 2018. On resistance of a rectangular thin plate under lateral indentation by a wedge indenter. *Ships Offshore Struct.* <https://doi.org/10.1080/17445302.2018.1441618>

Zhu L, Faulkner D. 1996. Damage estimate for plating of ships and platforms under repeated impacts. *Marine Struct.* 9(7):697–720.

Zhu L, Guo KL, Li YG, Yu TX, Zhou QW. 2018. Experimental study on the dynamic behavior of aluminum foam sandwich plates under single and repeated impacts at low temperature. *Int J Impat Eng.* 114:123-32.

Appendix

Jones assumed that the mass impactor has a negligible cross-section when compared with the plate dimensions (2012b). The radius of the impactor and the fully clamped circular plate (a) in this paper is 6mm and 37.5mm respectively. Therefore his theory for dynamic impacts is applicable in the scenarios of this study, and produces a response characterized by the transverse deformation profile in Fig. 21. The transverse velocity can be written as

$$\dot{v} = \frac{V_0}{\alpha(1+1/3\gamma)} \sin \alpha t - H \tag{A.1}$$

Where, \dot{v} is the transverse velocity of the plate field underneath the impactor.

To find a theoretical solution for Eq. (2), the initial condition is in the form of $w = 0$ and $\dot{v} = \frac{V_0}{\alpha(1+1/3\gamma)}$ in order to satisfy the conservation of linear momentum at $t=0$.

Thus, Eq. (2) has the general solution,

$$W = H \cos \alpha t + \frac{V_0}{\alpha(1+1/3\gamma)} \sin \alpha t - H \tag{A.2}$$

The plate ceases to move when $\dot{v} = 0$. Finally, Eq. (A.2) gives the dimensionless maximum transverse displacement, or the permanent deformation,

$$\frac{W_f}{H} = \sqrt{1 + \frac{3\gamma\Omega(1+6\gamma)}{2\pi(1+3\gamma)^2}} - 1 \tag{A.3}$$

Since the mass ratio γ of the experiments in this paper is 81.9 which means $\gamma \gg 1$, the Eq. (A.3) then reduces to Eq. (4)

Now Eq. (4) could be regarded as the resulting permanent deformation after the first impact. During the experiments, the second impact occurs after the first impact has ceased, and each has the same exact impact energy of 60J. Therefore the final deformation status of the first impact can be considered as the initial condition of the second impact whereas the initial velocity keeps the same, where $V = V_0(1 + 1/3\gamma)$ and $W = W_{f1}$. At the same time, resetting the time to $t=0$ at the start of the second impact.

The general solution for Eq. (2) with the initial conditions of the second impact is then derived as

$$W_2 = (W_{f1} + H) \cos \alpha t + \frac{V_0}{\alpha(1+1/3\gamma)} \sin \alpha t - H \quad (\text{A.4})$$

The dimensionless maximum permanent transverse displacement for the second impact when motion ceases is

$$\frac{W_{f2}}{H} = \sqrt{1 + \frac{3\gamma\Omega(1+6\gamma)}{2\pi(1+\Omega/\pi)(1+3\gamma)^2}} \times \left(\frac{W_{f1}}{H} + 1 \right) - 1 \quad (\text{A.5})$$

Similarly, when $\gamma \gg 1$ the Eq. (A.5) can be reduced to

$$\frac{W_{f2}}{H} = \sqrt{1 + \frac{2\Omega}{\pi}} - 1 \quad (\text{A.6})$$

Moreover, after the n th impacts, the dimensionless permanent transverse displacement turns out to be Eq. (6).

Table Captions

Table 1. Mechanical properties of AA5083-H116.

Table 2. Details of drop tests (The aluminum plates are circular with a diameter of 75mm).

Tables

Table 1

Mechanical properties of AA5083-H116.

Density [kg/m ³]	Young's modulus E[GPa]	Yield strength [MPa]	Ultimate tensile stress [MPa]	Poisson's ratio	Rupture strain
700	68	238	433	0.3	0.19

Table 2

Details of drop tests (The aluminum plates are circular with a diameter of 75mm).

<i>Test ID</i>	<i>L</i> (mm)	<i>L/2R</i>	<i>D</i> (mm)	<i>D/H</i>	<i>Notes</i>
B-0	0	0	0	0	Intact plate
B-1	8	2/3	1	1/6	Base case crack
L-1	2	1/6	1	1/6	
L-2	4	1/3	1	1/6	
L-3	6	1/2	1	1/6	
L-4	8	2/3	1	1/6	Same as B-1
L-5	12	1	1	1/6	
L-6	16	4/3	1	1/6	
D-1	8	2/3	1	1/6	Same as B-1
D-2	8	2/3	3	1/2	
D-3	8	2/3	6	1	

Figure Captions

Fig. 1. Tensile test coupons: (a) standard test pieces (ASTM E8); (b) dimensions (unit: mm).

Fig. 2. Measured stress-strain curves of AA5083-H116: (a) engineering stress-strain curve and true stress-strain curve; (b) fitting curve of true stress-plastic strain compared to experimental data points.

Fig. 3. A specimen with a surface crack (It is fastened to the support frame through the twelve bolts).

Fig. 4. Schematic diagram of crack prefabrication.

Fig. 5. Making of surface crack (a) general view; (b) partial enlarged view.

Fig. 6. The impact testing rig.

Fig. 7. Schematic diagram of impact test (The strong support/clamp frame has a circular opening in the middle).

Fig. 8. The deformation measurement set-up.

Fig. 9. Intact specimen under repeated impacts: (a) Time history of impact force; (b) Impact force-displacement curves.

Fig. 10. Deformed shape profile of intact specimen after each impact.

Fig. 11. The impact damage of intact specimen.

Fig. 12. Maximum impact force versus impact numbers (Test L-1 to L-6).

Fig. 13. Impact force-displacement curves at different impact numbers: (a) 1st impact; (b) 3rd impact; (c) 6th impact; (d) 8th impact.

Fig. 14. Post-impact images of L-Series.

Fig. 15. Maximum impact force versus impact numbers (Test D-1 to D-3).

Fig. 16. Impact force-displacement curves at different impact numbers: (a) 1st impact; (b) 3rd impact; (c) 5th impact; (d) 7th impact.

Fig. 17. Post-impact images of D-Series.

Fig. 18. Images of the surface with initial cracks (D-Series): (a) Specimen of $D/H = 1/6$; (b) Specimen of $D/H = 1/2$; (c) Specimen of $D/H = 1$.

Fig. 19. Comparisons between the theoretical predictions (curves) and experimental results (points) of the dimensionless maximum deformations of the intact plate (B-0) under repeated impacts.

Fig. 20. Maximum dimensionless deformations of plates with surface cracks (a) of different lengths (L-Series); (b) of different depths (D-Series).

Fig. 21. Assumed transverse displacements for a rigid, perfectly plastic circular plate struck at the center (a) plan view; (b) side view.

Figures

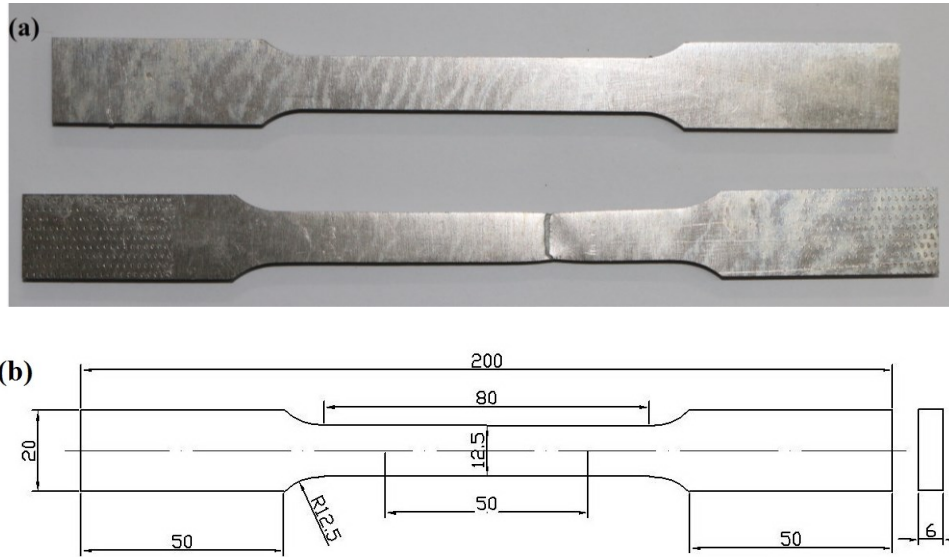


Fig. 1. Tensile test coupons: (a) standard test pieces (ASTM E8); (b) dimensions (unit: mm).

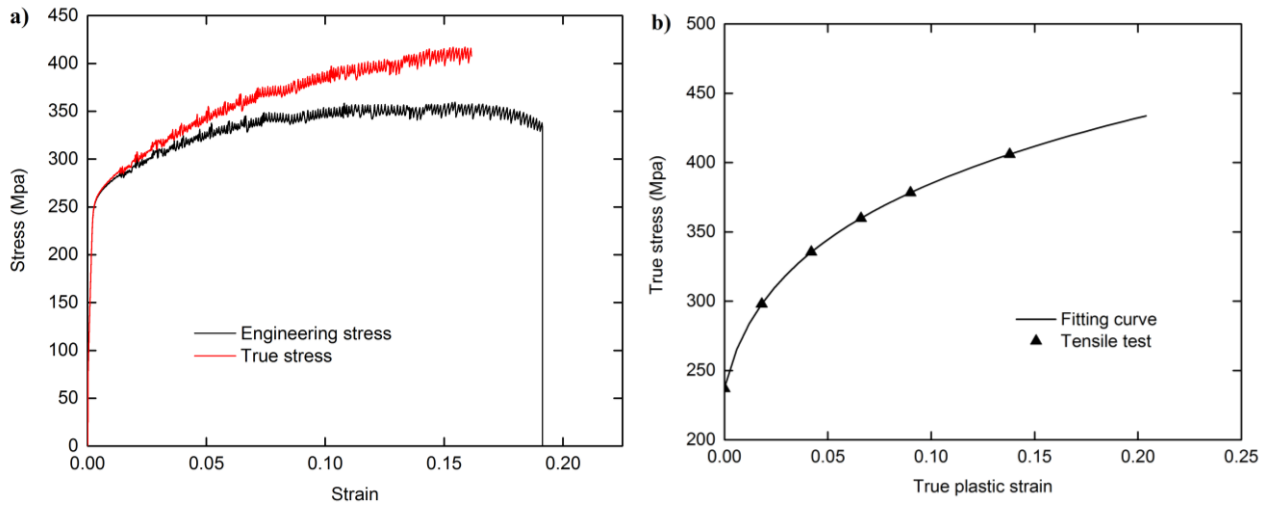


Fig. 2. Measured stress-strain curves of AA5083-H116: (a) engineering stress-strain curve and true stress-strain curve; (b) fitting curve of true stress-plastic strain compared to experimental data points.

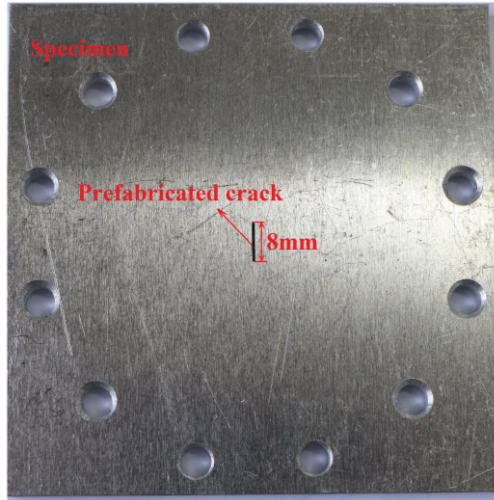


Fig. 3. A specimen with a surface crack (It is fastened to the support frame through the twelve bolts).

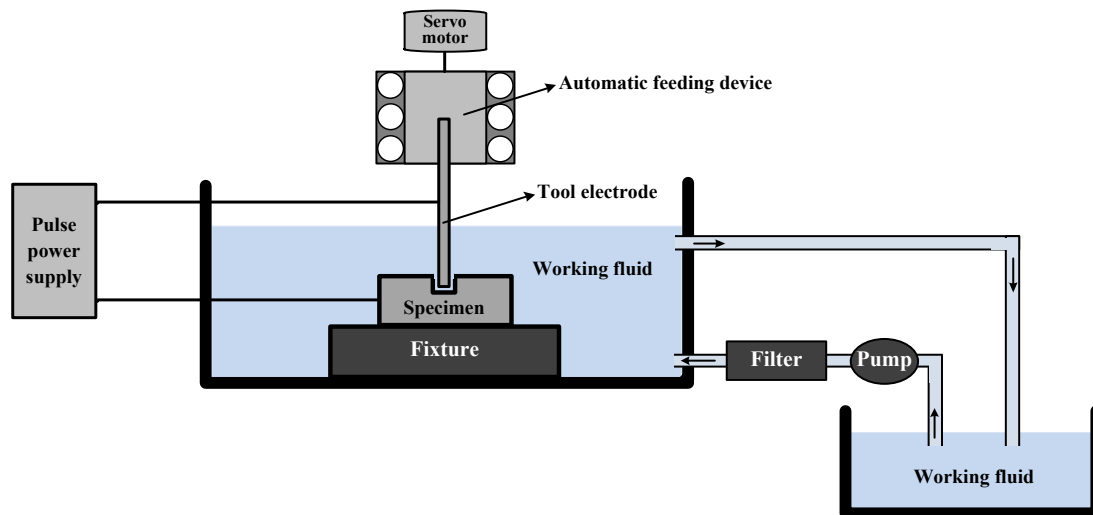


Fig. 4. Schematic diagram of crack prefabrication.

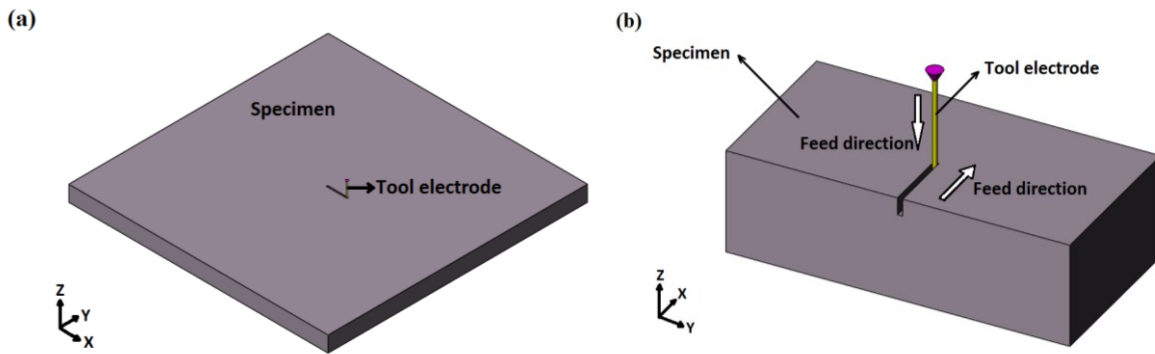


Fig. 5. Making of surface crack (a) general view; (b) partial enlarged view.

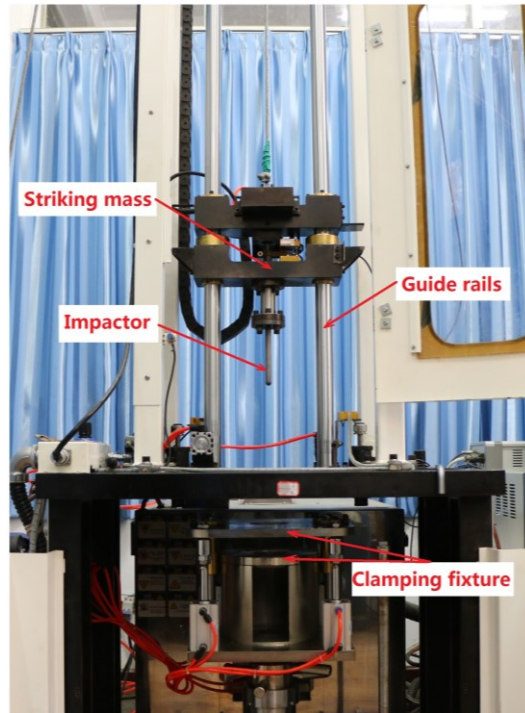


Fig. 6. The impact testing rig.

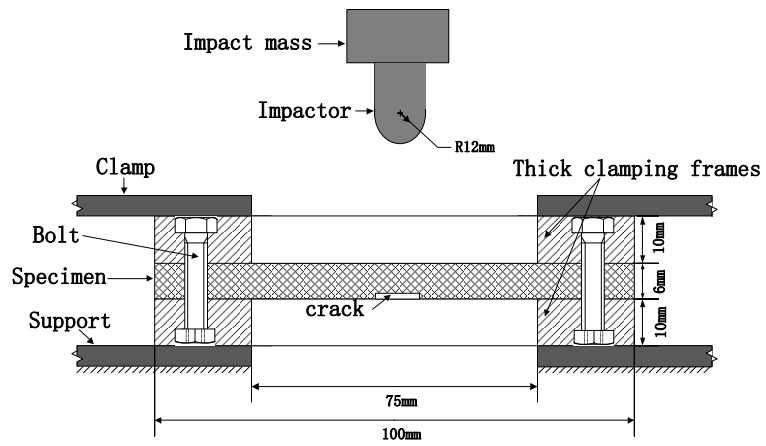


Fig. 7. Schematic diagram of impact test (The strong support/clamp frame has a circular opening in the middle).

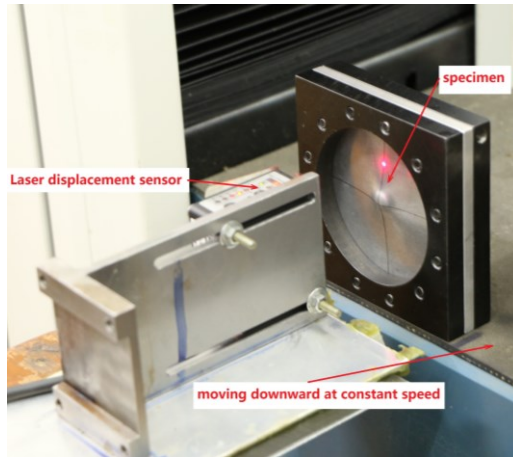


Fig. 8. The deformation measurement set-up.

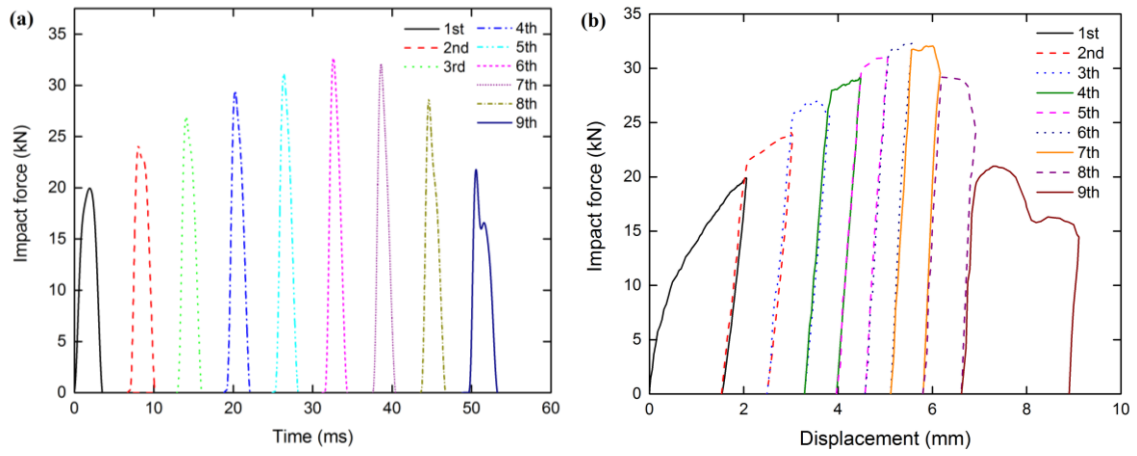


Fig. 9. Intact specimen under repeated impacts: (a) Time history of impact force; (b) Impact force-displacement curves.

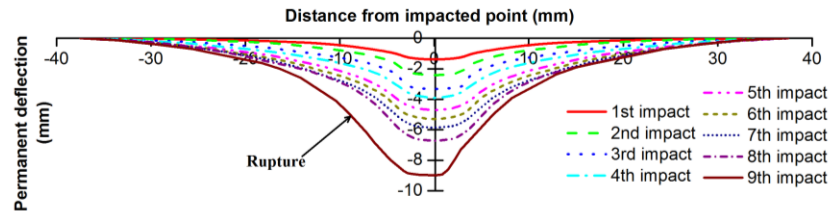


Fig. 10. Deformed shape profile of intact specimen after each impact.

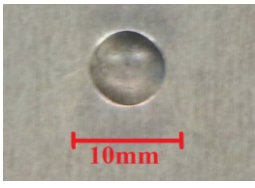
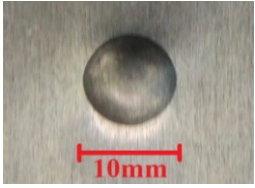
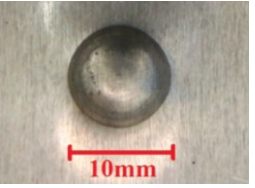
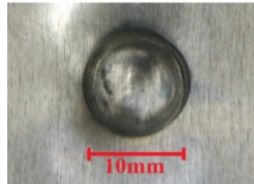
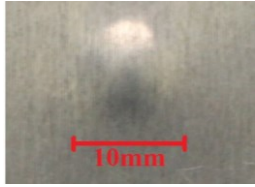
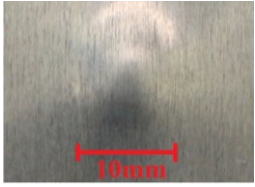
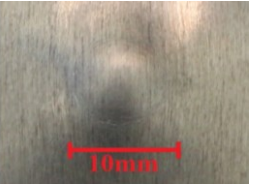
Impact no.	1 st	3 rd	6 th	9 th
Front surface				
Rear surface				

Fig. 11. The impact damage of intact specimen.

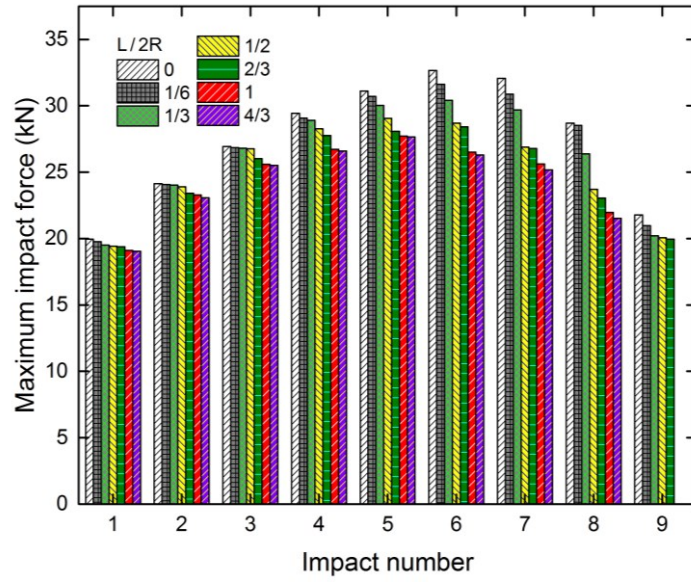


Fig. 12. Maximum impact force versus impact numbers (Test L-1 to L-6).

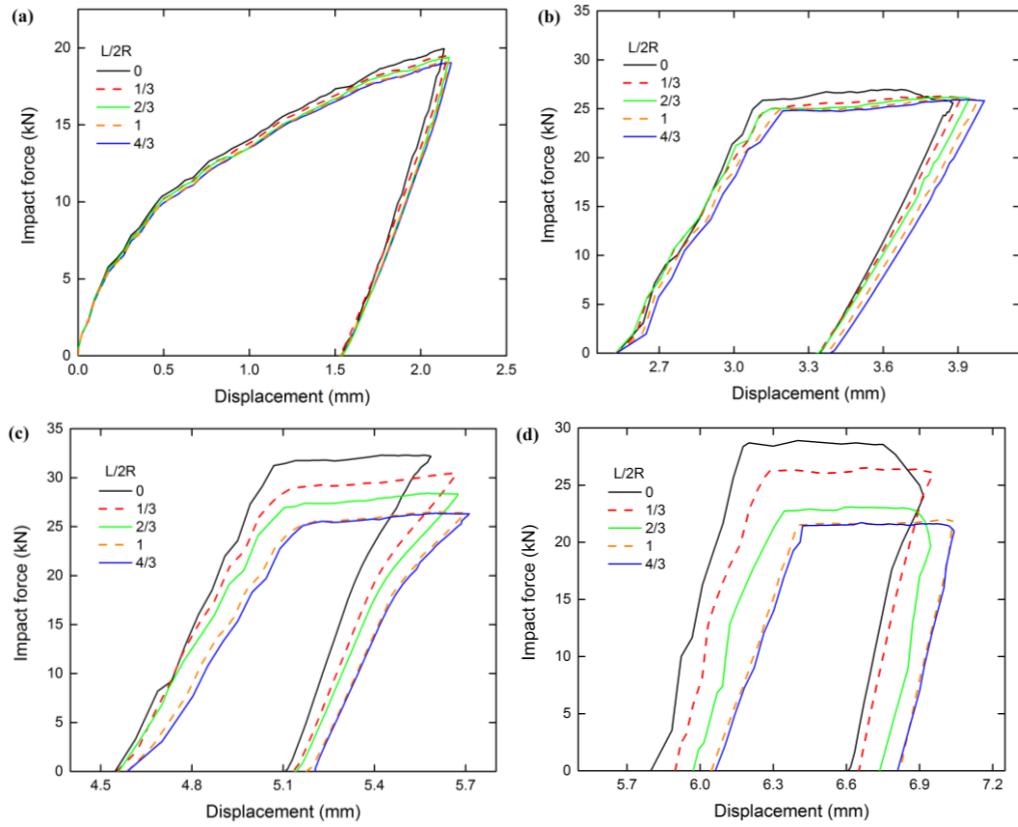


Fig. 13. Impact force-displacement curves at different impact numbers: (a) 1st impact; (b) 3rd impact; (c) 6th impact; (d) 8th impact.

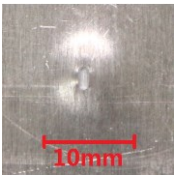
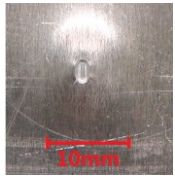
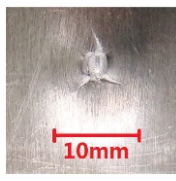
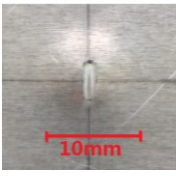
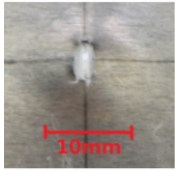
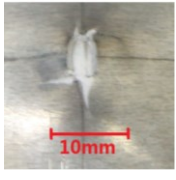
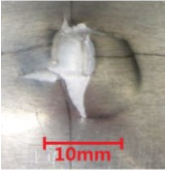
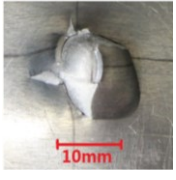
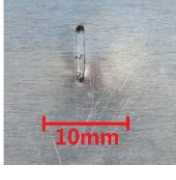
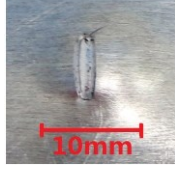
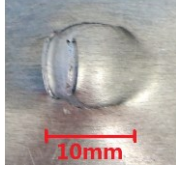
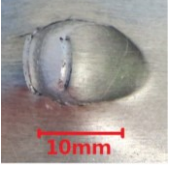
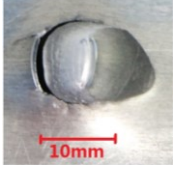
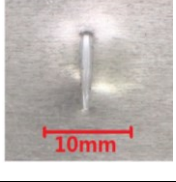
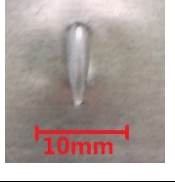
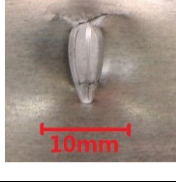
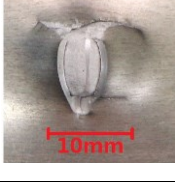
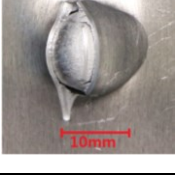
<i>L/2R</i>	1 st impact	3 rd impact	6 th impact	8 th impact	9 th impact
1/6					
1/3					
1/2					
2/3					
1					—
4/3					—

Fig. 14. Post-impact images of L-Series.

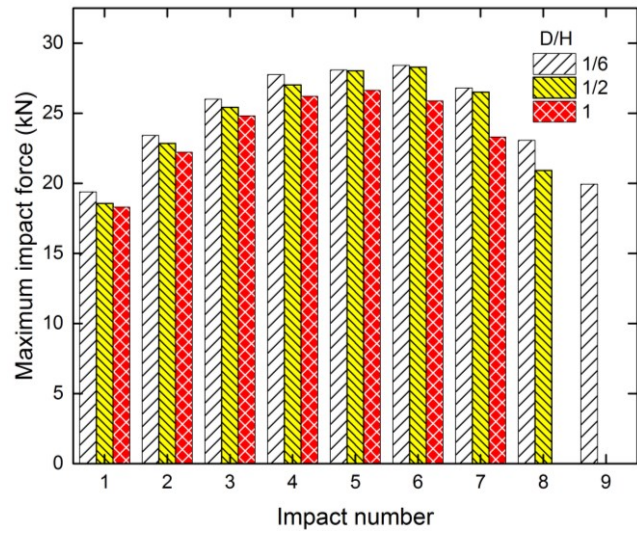


Fig. 15. Maximum impact force versus impact numbers (Test D-1 to D-3).

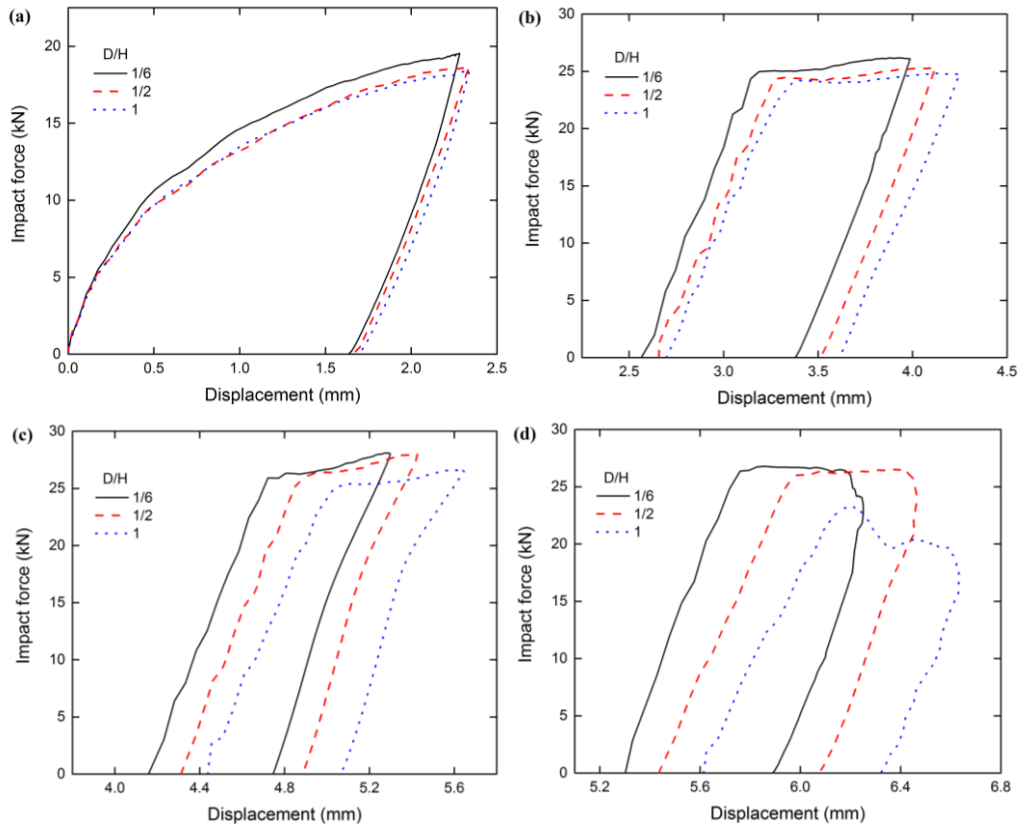


Fig. 16. Impact force-displacement curves at different impact numbers: (a) 1st impact; (b) 3rd impact; (c) 5th impact; (d) 7th impact.

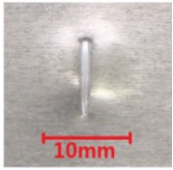
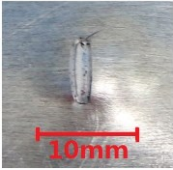
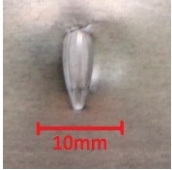
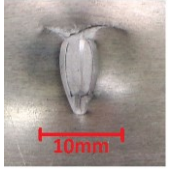
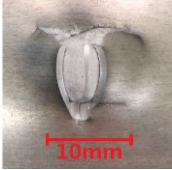
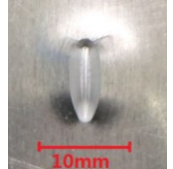
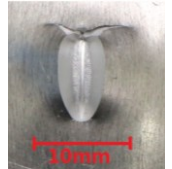
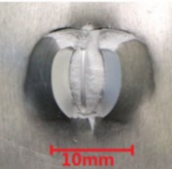
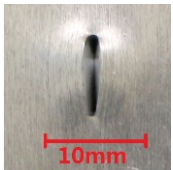
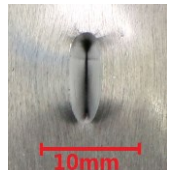
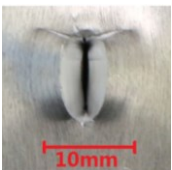
D/H	1 st impact	3 rd impact	5 th impact	7 th impact	8 th impact
1/6					
1/2					
1					—

Fig. 17. Post-impact images of D-Series.

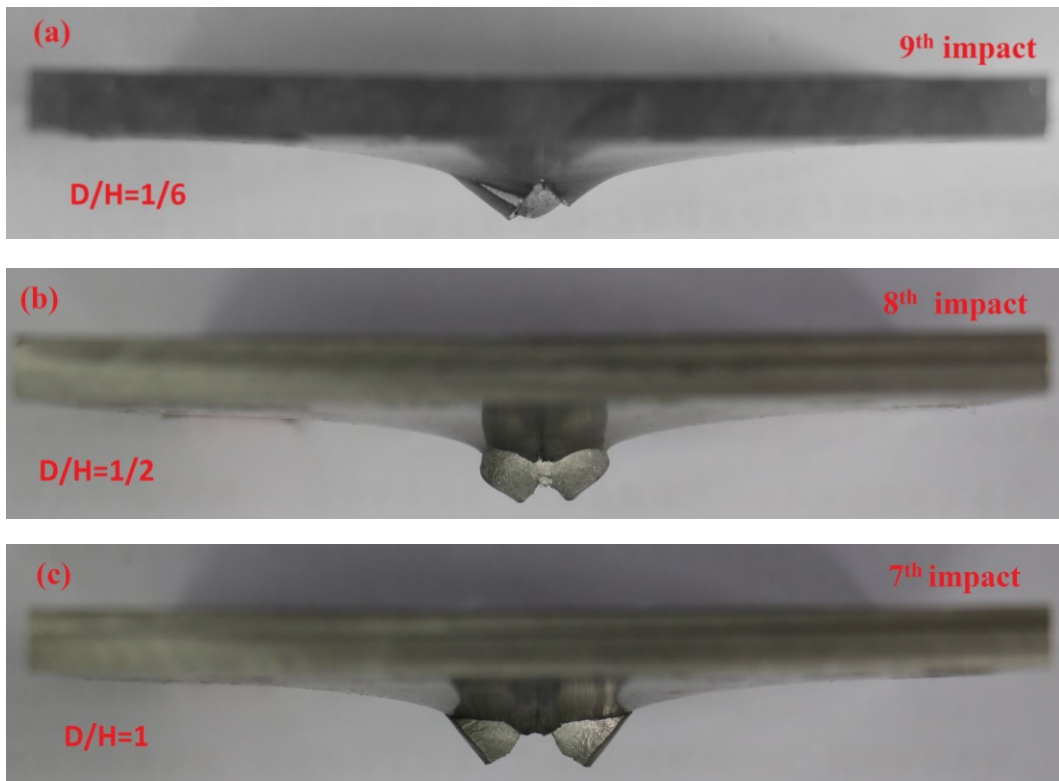


Fig. 18. Images of the surface with initial cracks (D-Series): (a) Specimen of $D/H = 1/6$; (b) Specimen of $D/H = 1/2$; (c) Specimen of $D/H = 1$.

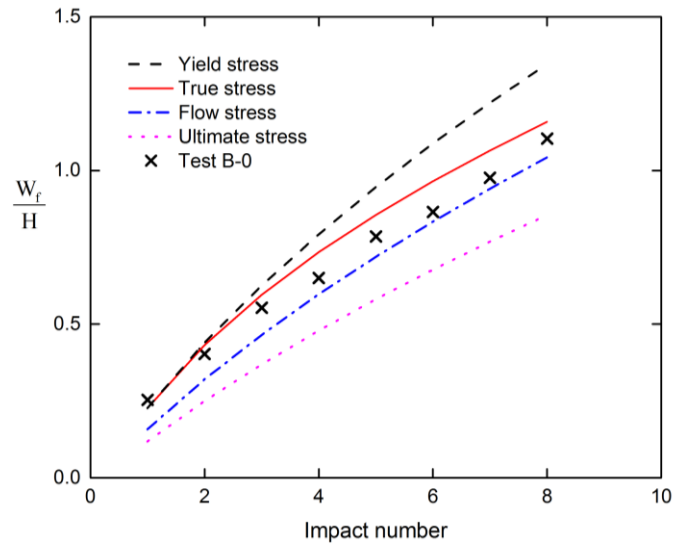


Fig. 19. Comparisons between the theoretical predictions (curves) and experimental results (points) of the dimensionless maximum deformations of the intact plate (B-0) under repeated impacts.

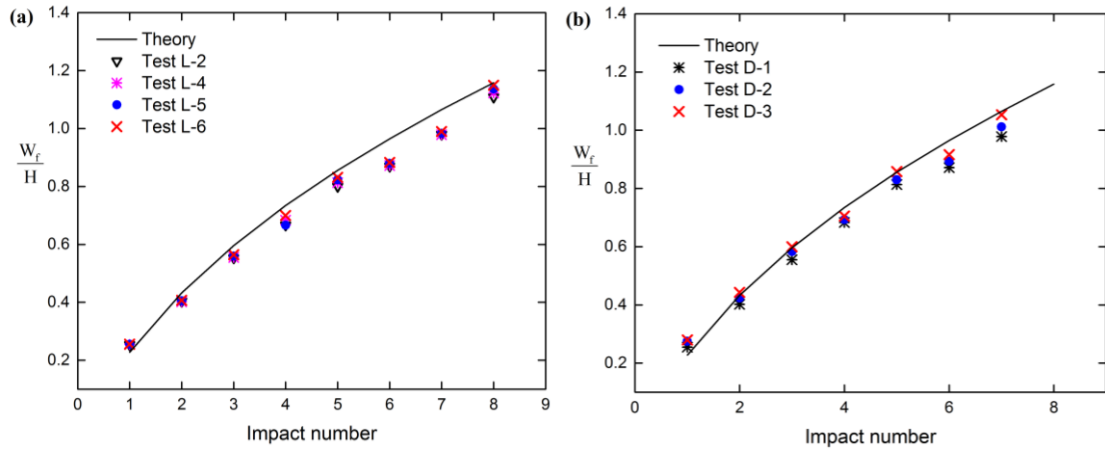


Fig. 20. Maximum dimensionless deformations of plates with surface cracks (a) of different lengths (L-Series); (b) of different depths (D-Series).

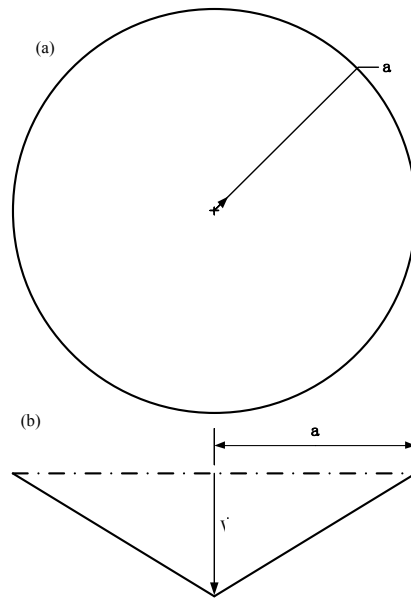


Fig. 21. Assumed transverse displacements for a rigid, perfectly plastic circular plate struck at the center (a) plan view; (b) side view.